Journal of Hazardous Materials 445 (2023) 130623

Contents lists available at ScienceDirect

Journal of Hazardous Materials

journal homepage: www.elsevier.com/locate/jhazmat

Atmospheric $PM_{2.5}$ induce autophagy and autophagic flux blockage in HUVEC cells via ROS/TXNIP signaling: Important role of metal components

Yan-yang Lu [a], Meiyi Cao [a,b], Fuping Li [a], Meiping Tian [a], Hongyun Ren [a], Qiaoqiao Chi [a], Qingyu Huang [a,*]

[a] Key Lab of Urban Environment and Health, Institute of Urban Environment, Chinese Academy of Sciences, Xiamen 361021, China
[b] College of Environmental and Safety Engineering, Fuzhou University, Fuzhou 10386, China

HIGHLIGHTS

- $PM_{2.5}$ induced autophagosome initiation and inhibited autophagic degradation.
- $PM_{2.5}$-bound metals were largely responsible for abnormal autophagy in HUVECs.
- ROS promoted autophagosome formation by positively regulating TXNIP.
- It was ROS, not TXNIP, that inhibited autophagic degradation in $PM_{2.5}$-exposed cells.

GRAPHICAL ABSTRACT

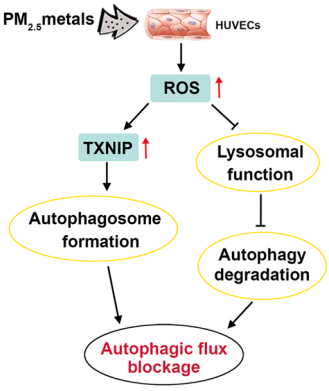

ARTICLE INFO

Editor: S. Nan

Keywords:
Water-extracted $PM_{2.5}$ (WE-$PM_{2.5}$)
Metals
Autophagy
Lysosome
Thioredoxin-interacting protein (TXNIP)

ABSTRACT

Autophagy was involved in vascular endothelial injury caused by $PM_{2.5}$, which aggravated the pathogenesis of cardiovascular diseases. However, major toxic components and underlying mechanism responsible for $PM_{2.5}$-induced autophagy remain unclear. In this study, the effects of water-extracted $PM_{2.5}$ (WE-$PM_{2.5}$) on autophagy in human umbilical vein endothelial cells (HUVEC) were studied. Our results showed WE-$PM_{2.5}$ promoted autophagosome initiation and formation, meanwhile, lysosomal function was impaired, which further caused autophagic flux blockage in HUVEC cells. Furthermore, removal of metals alleviated WE-$PM_{2.5}$-induced autophagic flux blockage, while the artificial metal mixture reproduced the WE-$PM_{2.5}$ response. Mechanistically, ROS regulated autophagy-related proteins evidenced by BECN1, LC3B and p62 expression reversed by NAC pretreatment in WE-$PM_{2.5}$-exposed cells. WE-$PM_{2.5}$ also increased TXNIP expression mediated by ROS; moreover, knockdown of TXNIP in WE-$PM_{2.5}$-exposed cells decreased BECN1 and LC3B expression, but had little effects on the expression of p62, CTSB, and CTSD, indicating WE-$PM_{2.5}$-induced TXNIP was involved in autophagosome initiation and formation rather than autophagic degradation. Collectively, WE-$PM_{2.5}$-induced ROS not only promoted autophagosome initiation and formation, but also inhibited autophagic degradation. However, as the

* Correspondence to: Institute of Urban Environment, Chinese Academy of Sciences, 1799 Jimei Road, Xiamen, 361021, China.
E-mail address: qyhuang@iue.ac.cn (Q. Huang).

https://doi.org/10.1016/j.jhazmat.2022.130623
Received 8 July 2022; Received in revised form 15 December 2022; Accepted 15 December 2022
Available online 17 December 2022

downstream molecule of ROS, TXNIP was only involved in autophagosome initiation and formation. Importantly, WE-$PM_{2.5}$-bound metals were largely responsible for autophagic flux blockage in HUVEC cells.

1. Introduction

Since outdoor air pollution, especially fine particulate matter ($PM_{2.5}$), was designated as a Group 1 carcinogen in 2013 by the International Agency for Research on Cancer (IARC) [40], the potential threat of $PM_{2.5}$ to public health has become topics of great international concern. Due to their small size and large specific surface area, the surface of atmospheric $PM_{2.5}$ can easily adsorb various pollutants in the air, including heavy metals (e.g., Cu, Zn, Mn, Co, Pb, and Cr), organic compounds (e.g., polycyclic aromatic hydrocarbons and their derivatives) and microorganisms (e.g., fungi, bacteria and viruses), which are harmful to human health [18,2,7]. Analysis from the global burden of diseases study revealed that the global deaths caused by ambient $PM_{2.5}$ has risen from 3.5 million in 1990 to 4.58 million in 2017, and the mortality continues to increase worldwide, especially in east and south Asia, thus placing ambient particulate matter pollution a top 10 risk factor [10,5,9]. Apart from the damage to respiratory system, the $PM_{2.5}$ largest threat to human health was to exacerbate the occurrence and development of cardiovascular diseases (CVD). A study of population data from 204 counties in the United States found that the risk of heart failure increased by 1.28 % per 10 $\mu g/m^3$ increase in $PM_{2.5}$ for short-term exposure [15], and for long-term exposure, each increase of 10 $\mu g/m^3$ $PM_{2.5}$ was strongly associated with a 14 % increase in stroke mortality and with a 16 % increase in mortality of ischaemic heart disease, these CVD risk still occurred even with $PM_{2.5}$ concentrations below the annual average standard of $PM_{2.5}$ in USA (12 $\mu g/m^3$) [23]. Therefore, the health hazards of $PM_{2.5}$ on cardiovascular system has occurred, and it is essential and meaningful to elucidate the underlying molecular mechanism and major toxic components responsible for ambient $PM_{2.5}$-trigged cardiovascular-associated diseases.

Vascular endothelial injury is the earliest pathophysiological basis contributing to $PM_{2.5}$-mediated CVD. The *in vitro* and *in vivo* studies confirmed that direct exposure to ambient $PM_{2.5}$ impaired the normal function of vascular endothelial cells, thereby aggravating the pathological process of CVD, in which autophagy dysfunction might play an important role [19,32,46,66]. As a dynamic metabolic process, autophagy (macroautophagy) involves in the sequestration of cargo in autophagosomes followed by degradation through the fusion of autophagosomes with lysosomes, which is critical for maintaining cellular homeostasis [27]. However, impairment of lysosomal function and blockage of autophagic flux disturb endothelial cell homeostasis and renewal in $PM_{2.5}$-exposed vein endothelial cells. For example, wang et al. confirmed that exposure to PM SRM1648a (a standard of atmospheric particulate matter) impaired the capacity of autophagic degradation, thereby blocking the autophagic flux in human umbilical vein endothelial cells (HUVEC) and EA. hy926 endothelial cells, which was caused by the impaired function of lysosomes, including lysosomal alkalization, destabilization and hydrolase inactivation; moreover, lysosomal associated membrane protein 2 (LAMP-2) was involved in the inhibition of autophagic flux [60,61]. However, the upstream molecular mechanism mediating $PM_{2.5}$-induced autophagic flux blockage has not been fully elucidated.

More importantly, due to the heterogeneity and complexity of real-world $PM_{2.5}$ samples, identifying the specific components which are associated with the induced cytotoxicity remains a serious challenge. Apart from the strong toxic effects of polycyclic aromatic hydrocarbons (PAHs) adsorbed by $PM_{2.5}$ [56,6,69], complex metals are also a class of potential toxic components which cannot be ignored. Both biological (cell-based) ROS assay and spectrophotometric cell-free assay fully proved that the $PM_{2.5}$-absorbed metals, especially transition metals (e.g., Cu, Zn, Cr, Fe, Ni, and Mn), were frequently and highly associated with ROS activity [50,57]. Furthermore, Ni interacting with other components of $PM_{2.5}$ induced endothelial dysfunction through systemic oxidative stress-dependent suppression of nitric oxide synthase 3 (eNOS) dimerization in a mouse model [68]. Consistently, Cuevas et al. selected two unique $PM_{2.5}$ samples that were similar in composition, but significantly different in the Ni concentration to study the endothelial injury in mice, and found that one of the $PM_{2.5}$ samples with 76-fold higher in the ambient level of Ni significantly increased the expression of vascular function marker VEGF (vascular endothelial growth factor A) and damaged acetylcholine-mediated vasorelaxation of microvessels [11]. Up to now, however, whether and which main metals absorbed in $PM_{2.5}$ trigger autophagy dysregulation and lysosomal damage in vascular endothelial cells remain unclear.

Oxidative stress injury is central in the pathophysiology of cardiovascular events through disturbance of vascular homeostasis. After entering the blood circulation, $PM_{2.5}$ can directly interact with vascular endothelial cells, thereby resulting in an imbalance of oxidative and antioxidant status with excessive production of reactive oxygen species (ROS) [39]. Furthermore, recent studies have pointed to an essential role for the accumulation of ROS in $PM_{2.5}$-mediated autophagy in HUVEC cells [12]. Thioredoxin interacting protein (TXNIP) is an oxidative- and inflammation-associated molecule. It is believed that TXNIP can be activated under oxidative stress status, thereby impairing the endothelial function and exacerbating CVD [13]. Notably, the emerging role of TXNIP in the regulation of autophagy has received great attention in the latest research. For example, decreased miR-146a-5p expression promoted autophagy and aggravated intestinal ischemia-reperfusion injury by negatively regulating TXNIP [36]. However, hyperglycemia-activated TXNIP inhibited autophagy and mitophagy in diabetic nephropathy via the mechanistic target of rapamycin kinase (mTOR) signaling pathway [26]. Interestingly, in a mouse model of myocardial ischaemia/reperfusion (I/R) injury, although inhibiting the autophagic degradation through increasing ROS levels, TXNIP increased autophagosome formation by directly interacting with Redd1, thereby contributing to I/R injury [17]. We speculate that TXNIP may be involved in $PM_{2.5}$-mediated autophagic process in vascular endothelial cells, which deserves further study.

Thus, in this study, major metals present in the real-world $PM_{2.5}$ samples collected from the urban area of Shanghai, China were either chelated/removed from the water-extracted $PM_{2.5}$, or reconstituted in an artificial metal mixture containing the similar composition and concentrations of the $PM_{2.5}$-bound metals for a complementary experiment, and the effect on autophagosome formation, autophagic degradation, lysosome function, ROS generation, as well as TXNIP expression were assessed in HUVEC cells. The objectives of this study are two-fold: (1) to identify and confirm the role of the main heavy metals adsorbed by $PM_{2.5}$ in autophagic flux blockage; (2) to reveal molecular mechanism regulating $PM_{2.5}$-induced abnormal autophagy in HUVEC cells through ROS and TXNIP.

2. Materials and methods

2.1. $PM_{2.5}$ sampling

The $PM_{2.5}$ sample was collected in Shanghai Academy of Environmental Sciences (31°10′N, 121°25′E) in the Yangtze River Delta region of China from November 6th to 17th, 2014. During the sampling period, the average concentration of $PM_{2.5}$ in Shanghai urban area was 66.08 $\mu g/m^3$, of which the highest concentration reached 137 $\mu g/m^3$. Pre-heated (500 °C, 4 h) quartz microfiber filters (203 mm × 254 mm, Whatman, UK) were used as the sampling medium to capture $PM_{2.5}$

using a high-volume sampler (TH-1000H, Wuhan Tianhong Instruments Co., Ltd., China) at a flow rate of 1.05 m^3 min^{-1}. The $PM_{2.5}$-enriched membranes were covered with aluminum foil, and stored at –20 ℃ until further analysis.

2.2. $PM_{2.5}$ extraction and chelate treatment

One eighth of each membrane was pooled together for extraction of water-soluble components. Briefly, $PM_{2.5}$ samples were cut into small pieces (3 cm × 3 cm), soaked in ultrapure water, and sonicated in an ice-water bath for 3 × 30 min. The collected $PM_{2.5}$ suspension was then filtered through 0.45 μm polypropylene syringe filters, dried by lyophilization and weighed. The water-soluble extracts were finally resuspended in sterilized water to achieve a stock concentration of 5 mg/mL (WE-$PM_{2.5}$). Blank quartz microfiber membranes were extracted with the same processing procedure for the control group.

To remove metals from water-soluble extracts of $PM_{2.5}$, an aliquot was processed through a solid-phase extraction (SPE) cartridge loaded with pre-cleaned Chelex 100 resin (Bio-Rad, #143–2832, USA) (hereinafter referred to as "Chel") as previous reported [47]. This chelated treatment could remove the vast majority of soluble metal cations and "loosely" bound metals from 50 μg/mL of WE-$PM_{2.5}$ [24,4,47].

2.3. Metal elements analysis

The WE-$PM_{2.5}$ and Chel solution was subjected to determine corresponding metal concentrations. Briefly, WE-$PM_{2.5}$ and Chel solutions were digested with a mixture of HNO_3 and HCl at 100 °C for 2 h, respectively. Subsequently, metallic elements in the digestion were measured by inductively coupled plasma mass spectrometry (ICP-MS; Agilent 7500cx, Agilent Technologies Incorporation, USA). Linear calibration curves were obtained from the standard solutions at 0.20, 0.50, 1.00, 10.00 and 50.00 ppb. Internal standards were Sc, Ge, Rh, and Lu, and the collision gas was helium. The coefficient of determination (R^2) was close to 1 (0.9970–1.0000) (Supplementary material: Table S1). Recovery efficiencies were calculated with blank quartz microfiber membranes spiked with the metallic elements of known concentrations. The results showed that recovery efficiencies obtained from each group of ten samples varied between 78.37 % and 118.43 % (Supplementary material: Table S2). The concentrations of 19 metal elements were shown in Table 1.

Table 1
Concentration of metals in water-soluble extract of $PM_{2.5}$ before and after metal chelation.

Elements	WE-$PM_{2.5}$ (μg/g)	Chel (μg/g)
Zn	3953.29 ± 22.93	13.46 ± 0.10
Al	3586.70 ± 88.08	306.88 ± 1.43
Fe	1928.55 ± 35.93	157.11 ± 0.78
Mn	530.09 ± 4.51	1.83 ± 0.03
Pb	247.91 ± 4.11	11.59 ± 0.04
Cr	177.15 ± 15.13	112.07 ± 0.82
Cu	167.45 ± 1.04	23.88 ± 0.10
Sr	97.40 ± 2.05	0.29 ± 0.02
Ba	72.34 ± 0.98	0.56 ± 0.02
V	63.98 ± 3.31	40.66 ± 0.04
As	53.49 ± 0.50	32.23 ± 0.58
Ni	43.95 ± 0.55	3.31 ± 0.01
Sn	32.82 ± 8.39	9.22 ± 1.55
Sb	28.94 ± 0.15	14.06 ± 0.03
Cd	21.25 ± 0.07	0.11 ± 0.01
Ti	15.52 ± 1.88	4.01 ± 0.14
Ga	10.91 ± 0.31	1.75 ± 0.09
Tl	7.23 ± 0.22	0.00 ± 0.01
Co	4.64 ± 0.07	0.55 ± 0.01

WE-$PM_{2.5}$: water-extract of $PM_{2.5}$; Chel: a solution obtained after removal of metals of WE-$PM_{2.5}$ by chelation. Data were expressed as the mean ± SEM.

2.4. An artificial metals mixture (AMM) preparation

To determine the effect of major metals on autophagy response, an artificial metals solution was prepared to mimic the concentrations of metals in WE-$PM_{2.5}$. The AMM was 11 metal elements with concentrations of more than 50 μg/g in the WE-$PM_{2.5}$ sample, including (1) major redox-active transition metals [Fe, Mn, Cr, Cu, V], (2) major non-redox-active metals [Zn, Al, Sr, Ba], (3) an important component of roadway emissions [Pb] and (4) a toxic non-metallic element widely present in the natural environment [As]. High-purity individual compounds were used to prepare the AMM, which provided a similar exposure level to the major metal elements of WE-$PM_{2.5}$ (50 μg/mL). The pH of Ctrl, WE-$PM_{2.5}$ (50 μg/mL), AMM and Chel preparations was measured with a pH meter (Starter 3100/F, China), and the measured values were 6.96 ± 0.14, 4.40 ± 0.11, 4.74 ± 0.12, and 6.24 ± 0.22, respectively.

2.5. Cell culture, transfection, and $PM_{2.5}$ exposure

The human umbilical vein endothelial cells (HUVEC) were cultured in F-12K medium (Gibco, USA) supplemented with 10 % FBS, 0.1 mg/mL heparin and 0.03 mg/mL ECGS at 37 °C in a 5 % CO_2 humidified incubator. For $PM_{2.5}$ exposure, cells were treated with serial concentrations of WE-$PM_{2.5}$ (5, 25, and 50 μg/mL), or WE-$PM_{2.5}$ (50 μg/mL), Chel and AMM solutions for 48 h, respectively. For TXNIP knockdown, HUVEC cells were transfected with control siRNA or TXNIP siRNA (GenePharma, China) using Lipofectamine™ 3000 transfection reagent (Invitrogen, USA) following exposure to 50 μg/mL of WE-$PM_{2.5}$ for 48 h. For detection of autophagic flux, cells were pretreated with 10 μM chloroquine (CQ, MedchemExpress, USA) for 2 h and then treated with WE-$PM_{2.5}$ (50 μg/mL), Chel, and AMM solutions for 48 h, respectively. In addition, to determine the effect of oxidative stress on WE-$PM_{2.5}$-induced autophagy, HUVEC cells were pretreated with an antioxidant N-acetyl cysteine (NAC, 5 mM) for 4 h before exposure to WE-$PM_{2.5}$ (50 μg/mL).

2.6. Cell viability assay

HUVEC cells were seeded in 96-well plates and treated with different concentrations (5, 25, 50 and 100 μg/mL) of WE-$PM_{2.5}$. After a 48-h exposure, 3-(4,5-dimethyl-2-thiazolyl)-2,5-diphenyl-2-H-tetrazolium bromide (MTT, 5 mg/mL, 10 μL) was added to each well and incubated for 4 h. The resulting formazan crystals were then dissolved in dimethyl sulfoxide (DMSO), and the absorbance was measured at 490 nm using a microplate reader (Spark, Tecan, Switzerland).

2.7. Transmission electron microscope (TEM) observation

TEM-based observation was carried out to examine WE-$PM_{2.5}$-induced autophagosomes in HUVEC cells at the ultrastructural levels. After treatment, cells were fixed with 2.5 % glutaraldehyde for 4 h, and post-fixed with 1 % osmium acid for 1 h. The samples were then dehydrated in a graded ethanol series and acetone, and embedded in Spurr resin. Subsequently, cell ultrathin sections were obtained using an ultramicrotome (Leica UC7, Germany), followed by stained with only uranyl acetate. Finally, sections were imaged under a TEM (H-7650, Hitachi, Japan).

2.8. RNA isolation and RT-PCR assay

After treatment, total RNA was isolated using TRIzol (Thermo Scientifc, USA). The cDNA was then synthesized with a HiScript® III RT SuperMix (Vazyme, China). Subsequently, quantitative PCR was performed with a AceQ® Universal SYBR qPCR Master Mix (Vazyme) in a LightCycler®480 Instrument II (Roche, Basle, Switzerland). The procedure for PCR amplification was performed as follows: the initial denaturation for 5 min at 95 °C; 45 cycles of amplification for 15 s at

95 °C; annealing and extension for 30 s at 60 °C [21,22]. The mRNA levels of *TXNIP* were normalized to *β-actin* using $2^{-\Delta\Delta Ct}$ method [37]. The primer sequences were provided in Supplementary material: Table S3.

2.9. Western blot analysis

After various treatments, cells were lysed with RIPA buffer (Thermo Scientific) and the protein concentrations were then measured by a BCA Protein Assay Kit (Thermo Scientific). 40 μg of protein were subjected to gel electrophoresis and immunoblotted with primary antibodies against BECN1 (Abcam, #ab207612, 1:2000), microtubule associated protein 1 light chain 3 beta (LC3B) (Abcam, #ab192890, 1:2000), sequestosome 1 (p62) (Abcam, #ab109012, 1:10000), Cathepsin B (CTSB) (Cell Signaling Technology, #31718, 1:1000), Cathepsin D (CTSD) (Abcam, #ab75852, 1:2000), TXNIP (Cell Signaling Technology, #1:1000), or β-actin (Cell Signaling Technology, #4970, 1:2000).

2.10. Detection of autophagic flux

Visualization of autophagic flux through infection with mCherry-GFP-LC3 lentivirus were performed as previously described [41]. Briefly, HUVEC cells were initially infected with tandem mCherry-GFP-LC3 lentivirus (Zolgene Biotechnology Co., China; MOI: 10) for 24 h according to the manufacturer's protocol. After exposure to WE-$PM_{2.5}$ (50 μg/mL) with and without NAC pretreatment, Chel and AMM for 48 h, cells were fixed with 4 % paraformaldehyde for 15 min, and visualized under a confocal laser-scanning microscope (LSM880, Carl Zeiss, Germany). The number of autolysosomes and autophagosomes were determined through manual counting of red (red^+green^-) and yellow (red^+ $green^+$) puncta in five random fields from the merged micrographs, respectively.

2.11. Lysosome staining

LysoSenso Green DND-189 dye and LysoTracke Red DND-99 dye were used to monitor the acidification and size of lysosomes, respectively. The exposed cells were incubated for 30 min at 37 °C with 1 μM LysoSenso Green DND-189 dye (Invitrogen) and 50 nM LysoTracke Red DND-99 dye (Invitrogen), respectively. The stained live cells were immediately observed with a LSM 710 Laser Scanning Confocal Microscope (Zeiss, Jena, Germany). The fluorescence intensity per cell stained with LysoSenso Green DND-189 was quantified with an ImageJ software. The size of lysosomes per cell was shown as the relative values compared to the control group analyzed by an ImageJ software.

2.12. Detection of acid phosphatase activity

HUVEC cells were treated with WE-$PM_{2.5}$ (50 μg/mL), Chel and AMM for 48 h, respectively. Subsequently, cell culture supernatants were collected for the determination of acid phosphatase activity by using a commercial acid phosphatase assay kit (Nanjing Jiancheng, China) according to the manufacturer's protocols. Finally, each specific activity was normalized to the corresponding protein content.

2.13. Oxidative stress detection

Oxidative stress potential was measured by quantifying intracellular reactive oxygen species (ROS) levels, H_2O_2 content, and reduced glutathione (GSH)/oxidized glutathione (GSSG) ratio. Intracellular ROS was determined using a fluorescent probe, 2,7-dichlorofluorescein diacetate (DCFH-DA). After various treatments, HUVEC cells were loaded with 10 μM DCFH-DA (Beyotime, China) and incubated for 30 min at 37 ℃ according to the manufacturer's instructions. The fluorescent images were immediately photographed with a LSM 710 laser scanning confocal microscope (Zeiss, Jena, Germany), and the fluorescent intensity per cell was quantified by an ImageJ software. The content of H_2O_2, GSH, and GSSG in lysates were measured using the commercialized kits (Beyotime, China), and calculated by monitoring the absorbance with a microplate reader (Spark, Tecan, Switzerland) based on the manufacturer's instructions.

2.14. Statistical analysis

Mean ± standard error of mean (SEM) was applied to present the results. One-way analysis of variance (ANOVA) followed by least significance difference (LSD) test was employed for multiple comparison using SPSS19 software. Values of $p < 0.05$ or $p < 0.001$ were considered as statistical significance. At least three independent experiments were designed for each experiment.

3. Results

3.1. WE-$PM_{2.5}$ induced autophagosome formation and inhibited autophagic degradation in HUVEC cells

As shown in Fig. 1A, a 48-h exposure to WE-$PM_{2.5}$ at the concentrations of more than 25 μg/mL induced a considerable decrease in cell viability in HUVEC cells. With the exposure concentration reached 50 μg/mL, the decrease in cell viability showed highly significant difference ($p < 0.001$), compared to the control group. Thus, we chose 50 μg/mL of WE-$PM_{2.5}$ as the maximum exposure level in the following experiments. To determine the autophagic response in WE-$PM_{2.5}$-exposed HUVEC cells, the TEM-based analysis was performed to directly observe the accumulation of autophagic vacuoles. As shown in Fig. 1B, exposure to WE-$PM_{2.5}$ resulted in excessive formation of autophagosomes, evidenced by a noticeable increase in autophagic vacuoles with bilayer/multilayer membranes. Moreover, the protein expression of BECN1, the key indicator of autophagosome initiation, was significantly upregulated in response to 25 or 50 μg/mL of WE-$PM_{2.5}$ (Fig. 1C and D). Meanwhile, the protein expression of LC3B II that is lipidation of LC3B, another important protein marker for autophagosome formation, was increased in WE-$PM_{2.5}$-exposed cells, and the ratio of LC3B II/I was also increased in a concentration-dependent manner (Fig. 1C, E, and F). These results indicated that WE-$PM_{2.5}$ promoted the initiation and accumulation of autophagosomes in HUVEC cells. In addition, WE-$PM_{2.5}$ exposure also led to a significant increase in the protein expression of p62 (Fig. 1C and G), suggesting autophagic degradation was inhibited in WE-$PM_{2.5}$-exposed cells. Taken together, HUVEC cells underwent the initiation and formation of autophagosomes in response to WE-$PM_{2.5}$ accompanied by the inhibition of autophagic degradation.

3.2. Contribution of major metals to impaired autophagy response in WE-$PM_{2.5}$-exposed HUVEC cells

To better characterize the contribution of metals to WE-$PM_{2.5}$-induced autophagy response in HUVEC cells, we prepared four exposure solutions: (1) Ctrl, method blanks that performed the same processing procedure with blank quartz microfiber membranes; (2) WE-$PM_{2.5}$ (50 μg/mL), water-extracted $PM_{2.5}$ samples from Shanghai, China surrounded by commercial and residential areas; (3) Chel, which 50 μg/mL of WE-$PM_{2.5}$ was passed through a Chelex 100 resin-loaded column to chelate soluble metals and the removal efficiency for the detected metals of WE-$PM_{2.5}$ was up to 93.35 % (Table 1); and (4) AMM, an artificial metals mixture with similar concentrations of 11 major metals to those consist in 50 μg/mL of WE-$PM_{2.5}$. That is, we added two complementary experiments to explore the possible role of metals in the toxic effects of $PM_{2.5}$: (1) HUVEC cells were exposed to Chel solution, in which a vast majority of soluble metals was removed from the aqueous extracts of real-world $PM_{2.5}$ by chelation, and the autophagy response was compared to the WE-$PM_{2.5}$ exposure group; (2) The AMM solution which imitated the main metal components and concentrations in WE-$PM_{2.5}$

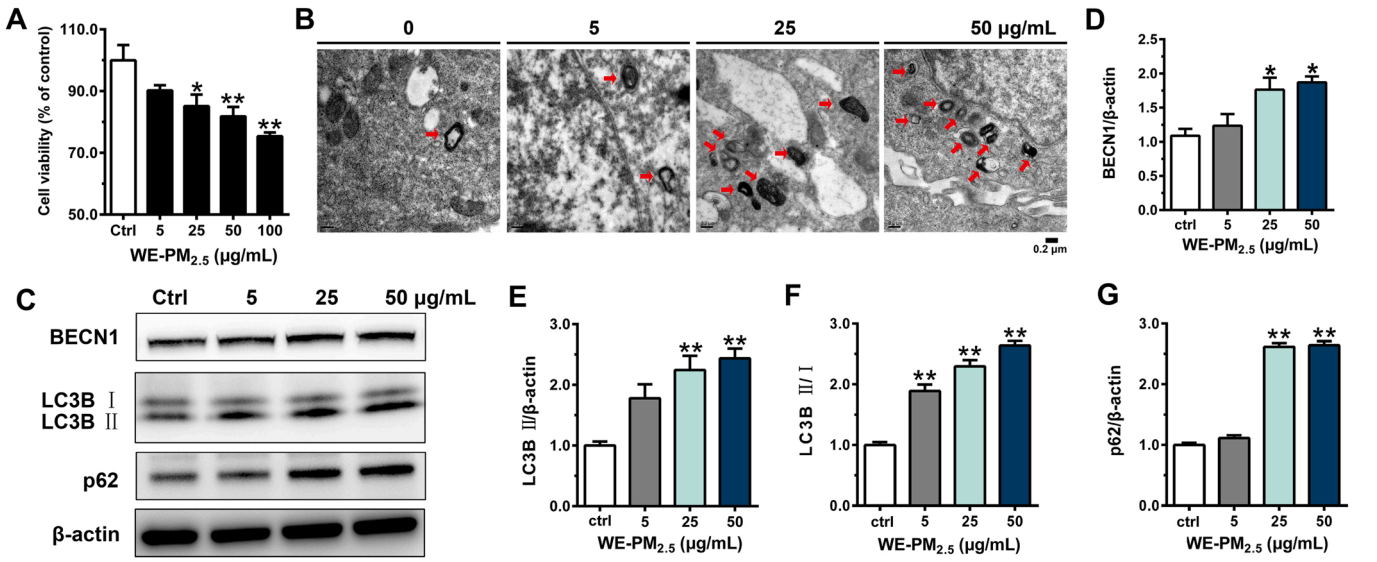

Fig. 1. Concentration-dependent effect of WE-$PM_{2.5}$ exposure on cell viability and autophagy in HUVEC cells. (A) cell viability detected by MTT assay. (B) Representative TEM images showing initial/degradative autophagic vacuoles (red arrows). Scale bar, 0.2 μm. (C) Western blot analysis of BECN1, LC3B I, LC3B II, and p62 protein. (D-G) Quantification of relative protein levels of BECN1(D), LC3B II (E), LC3B II/LC3B I (F) and p62 (G). HUVECs were treated with different concentrations of WE-$PM_{2.5}$ for 48 h, and the results were mean ± SEM from three independent experiments. * $p < 0.05$, ** $p < 0.001$ vs. controls.

was used to verify whether it could reproduce the response to WE-$PM_{2.5}$.

As shown in Fig. 2A, exposure to the metal-removed solution (Chel) resulted in a marked decrease in autophagosome-like structures compared to WE-$PM_{2.5}$ treatment. Conversely, the number of autophagic vacuoles was significantly increased in response to the AMM solution compared to control group. At the molecular level, we further confirmed that removal of metals by chelation remarkably diminished the elevated ratio of LC3B II/I, and the increased protein expression of BECN1, LC3B II, and p62 induced by 50 μg/mL of WE-$PM_{2.5}$, whereas exposure to AMM recapitulated the WE-$PM_{2.5}$ response to BECN1, LC3B and p62 in HUVEC cells (Fig. 2B-F), indicating metals were the major contributor to the initiation and accumulation of autophagosomes, as well as the blockage of autophagic degradation induced by WE-$PM_{2.5}$.

3.3. $PM_{2.5}$-bound metals blocked the autophagic flux in HUVEC cells

Actually, the autophagosomes accumulation was not only attributed to the activation of autophagosome formation, but also negatively related to autophagic degradation capacity. The above results confirmed the WE-$PM_{2.5}$-indued accumulation of autophagosomes was due to the

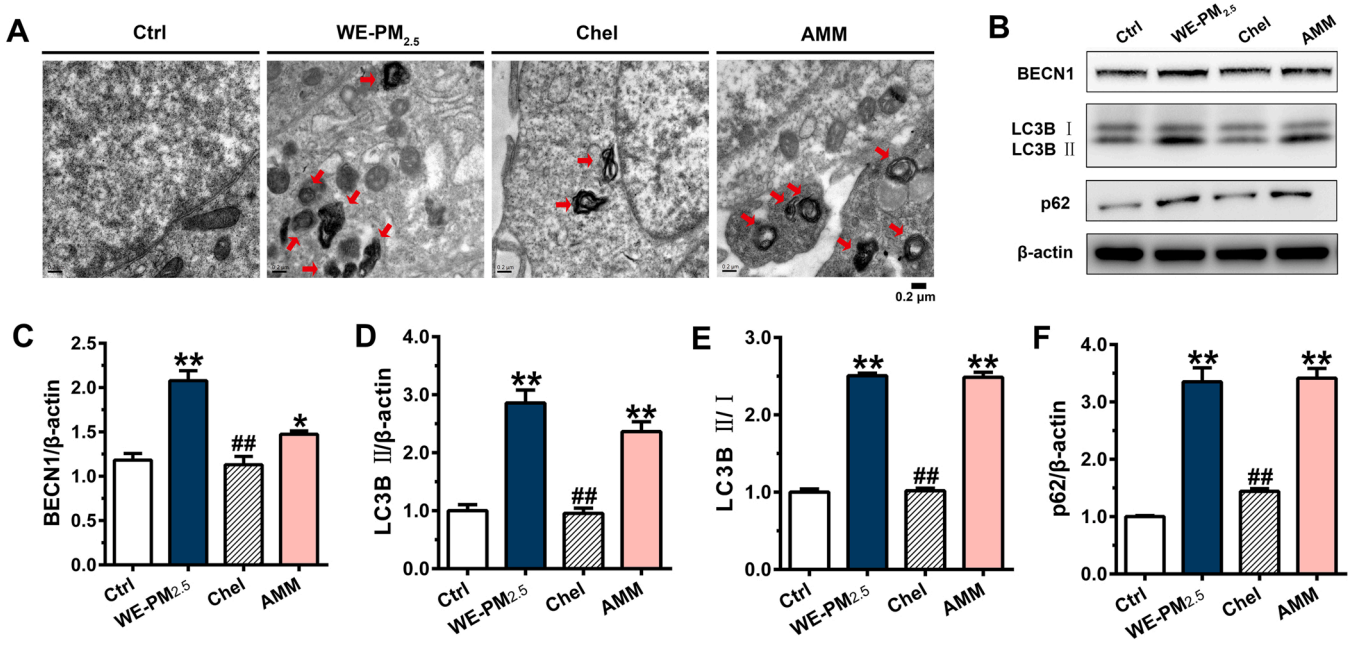

Fig. 2. Effect of WE-$PM_{2.5}$-bound metals on autophagosome formation and autophagic degradation in HUVEC cells. (A) Representative TEM images showing autophagosomes (red arrows). Scale bar, 0.2 μm. (B) Western blot analysis of BECN1, LC3B I, LC3B II, and p62 protein. (C-F) Quantification of relative protein levels of BECN1(C), LC3B II (D), LC3B II/LC3B I (E) and p62 (F). HUVECs were treated with 50 μg/mL of $PM_{2.5}$-water extract ("WE-$PM_{2.5}$"), a solution that chelates metals from $PM_{2.5}$-water extract ("Chel"), and another artificial metals mixture that mimics main metals of 50 μg/mL of $PM_{2.5}$-water extract ("AMM") for 48 h, respectively. The results were mean ± SEM from three independent experiments. * $p < 0.05$, ** $p < 0.001$ vs. controls. $^{\#\#}p < 0.001$ vs. WE-$PM_{2.5}$-treated cells.

activated vesicle nucleation in the process of autophagosome formation, evidenced by increased BECN1 protein expression. On the other hand, p62, a substrate of autophagy, seemed to be continuously accumulated without favorable degradation, which reflected that the process of autophagic flux might be inhibited to a certain extent in WE-$PM_{2.5}$-exposed HUVEC cells.

To determine the levels of autophagic flux, we treated HUVEC cells with WE-$PM_{2.5}$ (50 μg/mL), Chel and AMM solutions in the absence and presence of CQ (a late-stage autophagy inhibitor) for 48 h, respectively. The ratio of LC3B II protein expression with or without CQ in each treatment group was positively correlated with the corresponding level of autophagic flux. As shown in Fig. 3A and B, exposure to either WE-$PM_{2.5}$ or AMM solution caused a significant decrease in the levels of autophagic flux compared to the control group. Moreover, removal of most metals fully reversed autophagic flux level induced by WE-$PM_{2.5}$. Similarly, in the mCherry-GFP-LC3 lentivirus transfection assay, the number of autophagosomes (yellow puncta, $red^{+}green^{+}$) was prominently increased and autolysosomes (red puncta, $red^{+}green^{-}$) was remarkably decreased in HUVEC cells treated with the WE-$PM_{2.5}$ or AMM solution. Whereas autophagosomes and autolysosomes in Chel treatment recovered to a number close to that in control (Fig. 3C and D). These results confirmed that water-soluble extract of $PM_{2.5}$ blocked the autophagic flux in HUVEC cells, in this case metals were account for a large fraction of this effect.

3.4. $PM_{2.5}$-bound metals impaired lysosomal function in HUVEC cells

Lysosomes was a class of dynamic organelles participated in fusing with autophagosomes to form autolysosomes for subsequent cargo degradation. The structure and function of lysosomes directly determined whether the autophagy process could proceed smoothly. Lysosomal damage has been reported to inhibit the level of autophagic flux, thereby triggering autophagy dysfunction and preventing mammalian cells from self-renewal [51]. We, therefore, investigated the effect of $PM_{2.5}$ on lysosomal activity in HUVEC cells. A lysosome probe, LysoTracker Red DND-99, was performed to label acidic lysosomes in live HUVEC cells. The results showed the size of lysosomes was enlarged upon treatment with WE-$PM_{2.5}$ or AMM, suggesting lysosome swelling. However, there was no distinct change in Chel-treated cells (Fig. 4A and B). We next measured the lysosomal acidification using a pH-sensitive fluorescent dye, LysoSensor Green DND-189. As illustrated in Fig. 4C and D, there was a prominent enhancement in fluorescence intensity following exposure to WE-$PM_{2.5}$ and AMM, not Chel, which confirmed that $PM_{2.5}$-bound metals changed lysosomal microenvironment, characterized by enhanced acidity of lysosomes. The activity of acid phosphatase was also attenuated after WE-$PM_{2.5}$ and AMM exposure compared to control and enhanced under Chel exposure compared to WE-$PM_{2.5}$ exposure (Fig. 4E). CTSB and CTSD were two classical hydrolase proteins, which were vital for the degradation of cargo. As

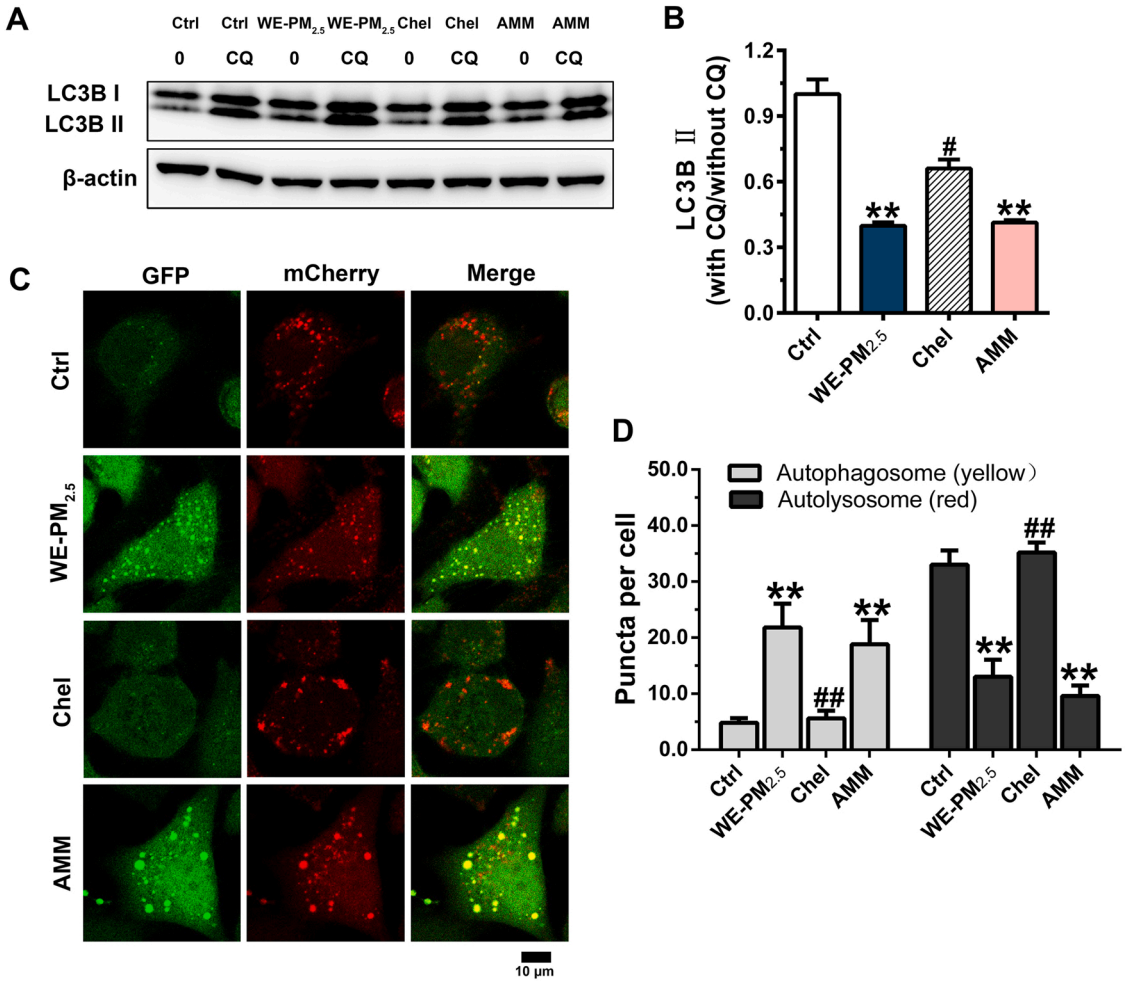

Fig. 3. WE-$PM_{2.5}$-bound metals blocked autophagic flux in HUVEC cells. (A)Western blot analysis of LC3B protein in HUVEC cells exposed to WE-$PM_{2.5}$, Chel, and AMM for 48 h with or without chloroquine (CQ, 10 μM) pretreatment. (B) The relative autophagic flux levels, represented as the protein expression of LC3B II (with CQ)/LC3B II (without CQ). (C) Representative images of mCherry-GFP-LC3 puncta in cells exposed to WE-$PM_{2.5}$, Chel, and AMM for 48 h, respectively. Scale bar, 10 μm. (D) Average number of autolysosomes (red dots) and autophagosomes (yellow dots) per cell. The results were mean ± SEM from three independent experiments. ** $p < 0.001$ vs. controls. $^{\#}p < 0.05$, $^{\#\#}p < 0.001$ vs. WE-$PM_{2.5}$-treated cells.

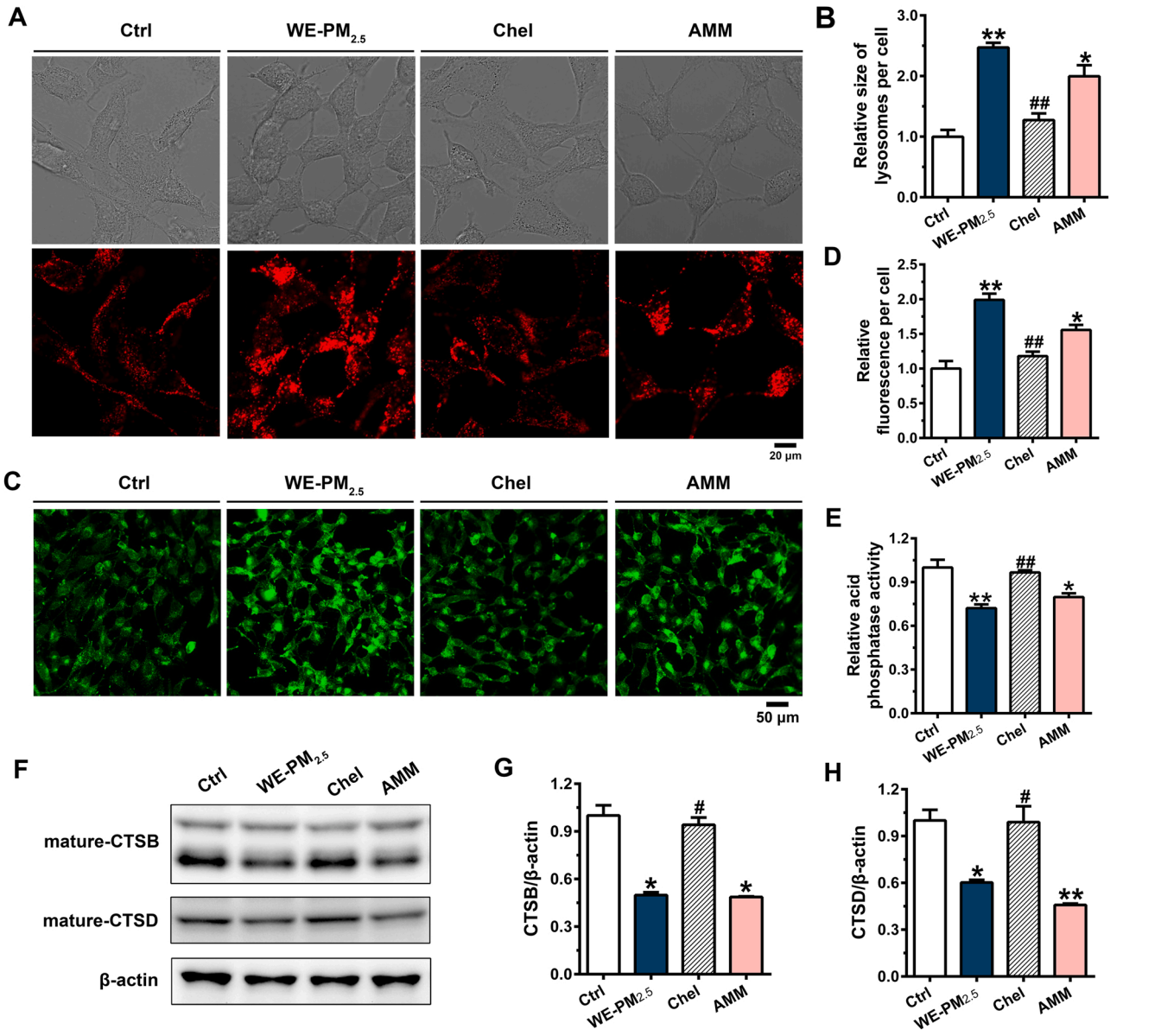

Fig. 4. WE-$PM_{2.5}$-bound metals impaired lysosomal activity in HUVEC cells. (A) Representative images of lysosomes in HUVECs stained by LysoTracker™ Red DND-99, showing the size of lysosomes. Scale bar, 20 μm. (B) Relative size of lysosomes per cell stained by LysoTracker™ Red DND-99. (C) Representative images of lysosomes in HUVEC cells stained by LysoSensor™ Green DND-189, showing the acidity of lysosomes. Scale bar, 50 μm. (D) Relative fluorescence intensity per cell stained by LysoSensor™ Green DND-189. (E) Acid phosphatase activity in culture supernatants. (F) Western blot analysis of CTSB and CTSD protein. (G and H) Quantification of relative protein levels of CTSB (G) and CTSD (H). HUVEC cells were treated with WE-$PM_{2.5}$, Chel, and AMM for 48 h, respectively. The results were mean ± SEM from three independent experiments. * $p < 0.05$, ** $p < 0.001$ vs. controls. $^{\#}p < 0.05$, $^{\#\#}p < 0.001$ vs. WE-$PM_{2.5}$-treated cells.

shown in Fig. 4F-H, the protein expression of mature CTSB and CTSD was significantly decreased in WE-$PM_{2.5}$-treated cells, which was parallel to the changes in AMM-treated cells, while Chel exposure completely reversed the expression of CTSB and CTSD induced by WE-$PM_{2.5}$. These data fully demonstrated that WE-$PM_{2.5}$ enhanced the acidity of lysosomal microenvironment, thereby impairing the normal function of lysosomes in HUVEC cells. Importantly, the metals played a key toxic effect in this biological process.

3.5. *Intracellular ROS mediated WE-$PM_{2.5}$-induced autophagy dysregulation in HUVEC cells*

Exposure to WE-$PM_{2.5}$ and AMM solution triggered an increase in the ROS and H_2O_2 production and a decrease in the GSH/GSSG ratio, while the negative control and Chel solution did not. Moreover, the addition of NAC (a ROS scavenger) reversed the increased levels of ROS and H_2O_2 and the reduced GSH/GSSG ratio induced by WE-$PM_{2.5}$ (Fig. 5A and B, Fig. S1A and B), suggesting $PM_{2.5}$-adsorbed metals could induce oxidative stress in HUVEC cells. We further investigated whether ROS could regulate autophagy in WE-$PM_{2.5}$-treated HUVEC cells by detecting autophagy-related proteins. As shown in (Fig. 5C-G), the NAC pretreatment remarkably reduced the protein expression of BECN1, LC3B II, and p62 compared to only WE-$PM_{2.5}$ exposure, indicating autophagosome formation and autophagic degradation were mediated to some extent by ROS levels following exposure to WE-$PM_{2.5}$. Furthermore, the function of lysosomes also depended on intracellular ROS levels, as evidenced by the protein expression of mature CTSB and CTSD effectively restored by NAC pretreatment in WE-$PM_{2.5}$-exposed cells (Fig. 5C, H and I). In mCherry-GFP-LC3 lentivirus transfection assay, the NAC pretreatment significantly decreased the number of autophagosomes

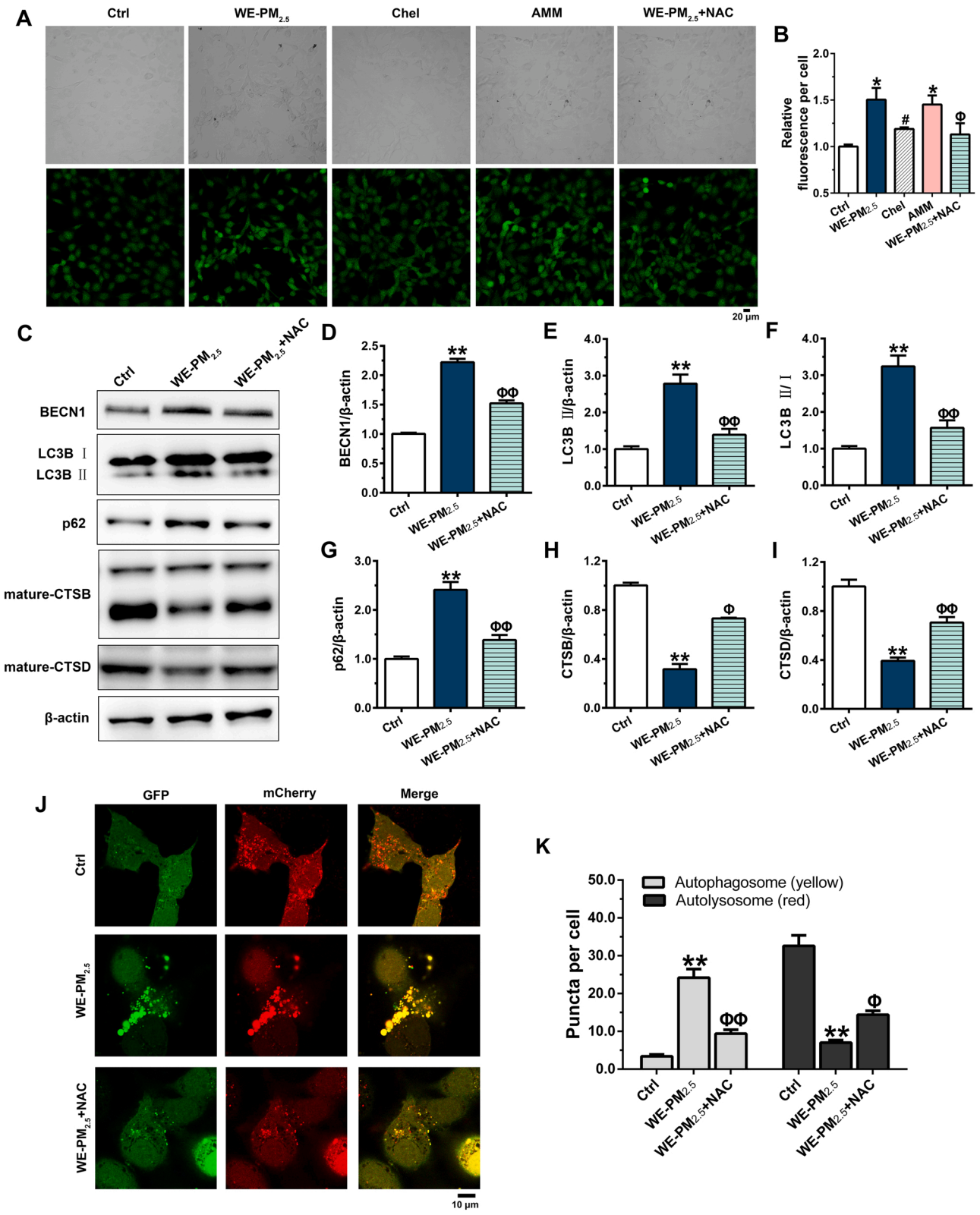

Fig. 5. WE-$PM_{2.5}$ exposure induced an increase of intracellular ROS generation in HUVEC cells, which was responsible for the impaired autophagy and lysosome function. (A) Representative micrographs of DCF fluorescence. Scale bar, 20 μm. (B) Relative quantitative analysis of fluorescence intensity per cell. Five micrographs per treatment were taken. (C) Western blot analysis of BECN1, LC3B I, LC3B II, p62, CTSB and CTSD protein. (D-I) Quantification of relative protein levels of BECN1 (D), LC3B II (E) LC3B II/LC3B I (F), p62 (G), CTSB (H) and CTSD (I). (J) Representative images of mCherry-GFP-LC3 puncta in cells exposed to WE-$PM_{2.5}$ (50 μg/mL) with and without NAC pretreatment, respectively. Scale bar, 10 μm. (K) Average number of autolysosomes (red dots) and autophagosomes (yellow dots) per cell. For A and B, cells were exposed to WE-$PM_{2.5}$ (50 μg/mL) with or without NAC (5 mM) pretreatment, Chel, and AMM, respectively; for C-I, cells were exposed to WE-$PM_{2.5}$ (50 μg/mL) with or without NAC pretreatment, respectively. The results were mean ± SEM from three independent experiments. * $p < 0.05$, ** $p < 0.001$ vs. controls. $^{\#}p < 0.05$ vs. WE-$PM_{2.5}$-treated cells. $^{\Phi}p < 0.05$, $^{\Phi\Phi}p < 0.001$ vs. WE.$PM_{2.5}$treated cells.

(yellow dots) and increased the autolysosomes (red dots) compared to the lone WE-$PM_{2.5}$ exposure, suggesting that inhibition of oxidative stress effectively reversed the autophagic flux blockage caused by WE-$PM_{2.5}$ in HUVEC cells (Fig. 5J and K). Taken together, WE-$PM_{2.5}$-induced ROS partly promoted the initiation and formation of autophagosomes, accompanied by the impairment of lysosomal function and inhibition of autophagic degradation, thereby resulting in the blockage of autophagic flux in HUVEC cells.

3.6. *TXNIP was involved in autophagosome formation, but not autophagic degradation in WE-$PM_{2.5}$-treated HUVEC cells*

Thioredoxin interacting protein (TXNIP), an oxidative stress-related molecule, plays a major role in regulation of redox homeostasis through inhibition of antioxidative function [14]. We, therefore, investigated the effect of WE-$PM_{2.5}$ exposure on TXNIP expression in HUVEC cells. As presented in Fig. 6A and B, the protein expression of TXNIP was concentration-dependently increased following exposure to WE-$PM_{2.5}$ for 48 h, and also increased in response to AMM solution, while TXNIP expression was restored to near-basal levels after removal of metals from WE-$PM_{2.5}$ in HUVEC cells (Fig. 6C and D). Furthermore, pretreatment with NAC effectively relieved WE-$PM_{2.5}$-induced protein expression of TXNIP (Fig. 6E and F), suggesting WE-$PM_{2.5}$-adsorbed metals induced an increase of TXNIP expression, which was mediated by intracellular ROS in HUVEC cells.

To further verify the interaction between TXNIP and autophagy in WE-$PM_{2.5}$-exposed cells, we transfected TXNIP siRNA to knockdown TXNIP expression in HUVEC cells. The transfection efficiency was verified by RT-PCR assay (Fig. 7A and B). Using this cell model, we found that inhibition of TXNIP expression effectively reversed WE-$PM_{2.5}$-activated protein expression of BECN1 and LC3B II, as well as the LC3B II/LC3B I ratio (Fig. 7C-F), indicating the initiation and formation of autophagosomes triggered by WE-$PM_{2.5}$ partly attributed to the activation of ROS-TXNIP signaling in HUVEC cells. Nevertheless, knockdown of TXNIP in WE-$PM_{2.5}$-exposed cells failed to induce a noticeable difference in the protein expression of p62 compared to only WE-$PM_{2.5}$ exposure (Fig. 7C and G), suggesting the activation of TXNIP caused by WE-$PM_{2.5}$ did not influence the capacity of autophagic degradation in HUVEC cells. Similarly, no significant differences in the protein expression of mature CTSB and CTSD were observed upon TXNIP knockdown, which confirmed that TXNIP might not be involved in the function of lysosomes in WE-$PM_{2.5}$-exposed HUVEC cells.

4. Discussion

An increasing amount of epidemiological and toxicological evidence has confirmed that $PM_{2.5}$ exposure impaired normal vascular endothelial function, thereby aggravating the pathogenesis of a series of cardiovascular-associated diseases, in which autophagy played an important role [32,48,61,63]. However, the upstream molecular mechanisms and major toxic components responsible for ambient $PM_{2.5}$-trigged autophagy dysregulation were not fully elucidated. In this study, HUVEC cells were used as a classic vascular endothelial cell model to explore the regulatory mechanism of ROS and TXNIP in $PM_{2.5}$-induced autophagic flux. Importantly, the toxic effects of $PM_{2.5}$-bound major metals on the blockage of autophagic flux were also confirmed, which added new knowledge to $PM_{2.5}$-related vascular endothelial injury.

Vascular endothelium throughout the inner lining of blood vessel wall is the first line to defense against external stimuli for the cardiovascular system [30]. When $PM_{2.5}$ entered the blood circulatory system through the alveoli, it would inevitably come into direct contact with vascular endothelial cells, and induced inflammation, oxidative stress, apoptosis and ferroptosis, thereby leading to endothelial dysfunction and aggravating the progression of CVD [39,48,58,62]. It is worth noting that more attention has been paid to the role of emerging autophagy in the toxic effects of $PM_{2.5}$. It has been reported that $PM_{2.5}$ could induce dysregulation of autophagy through endoplasmic reticulum stress, ultimately leading to endothelial cell apoptosis [63]. Autophagy (macroautophagy) is a lysosome-dependent degradation pathway to remove senescent or damaged organelles and maintain basal energy balance, including initiation and vesicle nucleation, vesicle elongation, fusion and degradation [27]. The complete process of autophagy is called autophagic flux. In this process, BECN1, LC3B and p62 are the most credible marker proteins used to assess the state of autophagy. BECN1 participates in the process of vesicle nucleation by forming PI3K

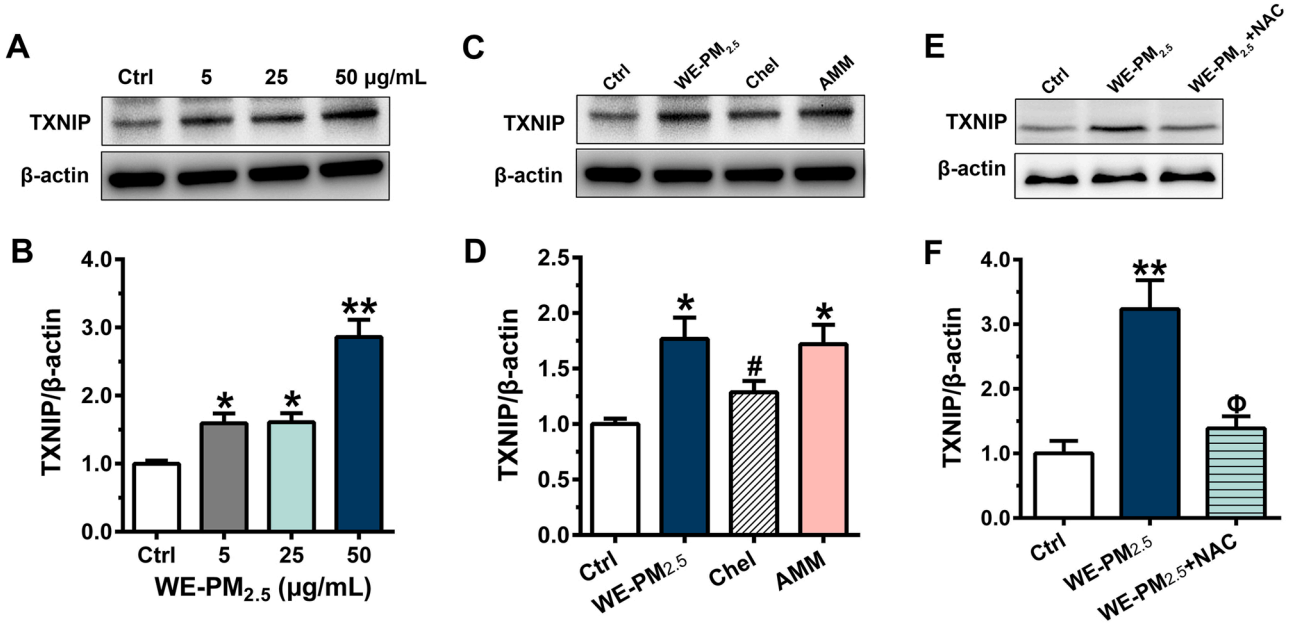

Fig. 6. WE-$PM_{2.5}$-bound metals upregulated the protein expression of TXNIP which was mediated by ROS. (A-F) Western blot analysis of TXNIP protein with different treatment, and corresponding quantification of TXNIP. * $p < 0.05$, ** $p < 0.001$ vs. controls. $^{\#}p < 0.05$ vs. WE-$PM_{2.5}$-treated cells. $^{\Phi}p < 0.05$ vs. WE-$PM_{2.5}$-treated cells.

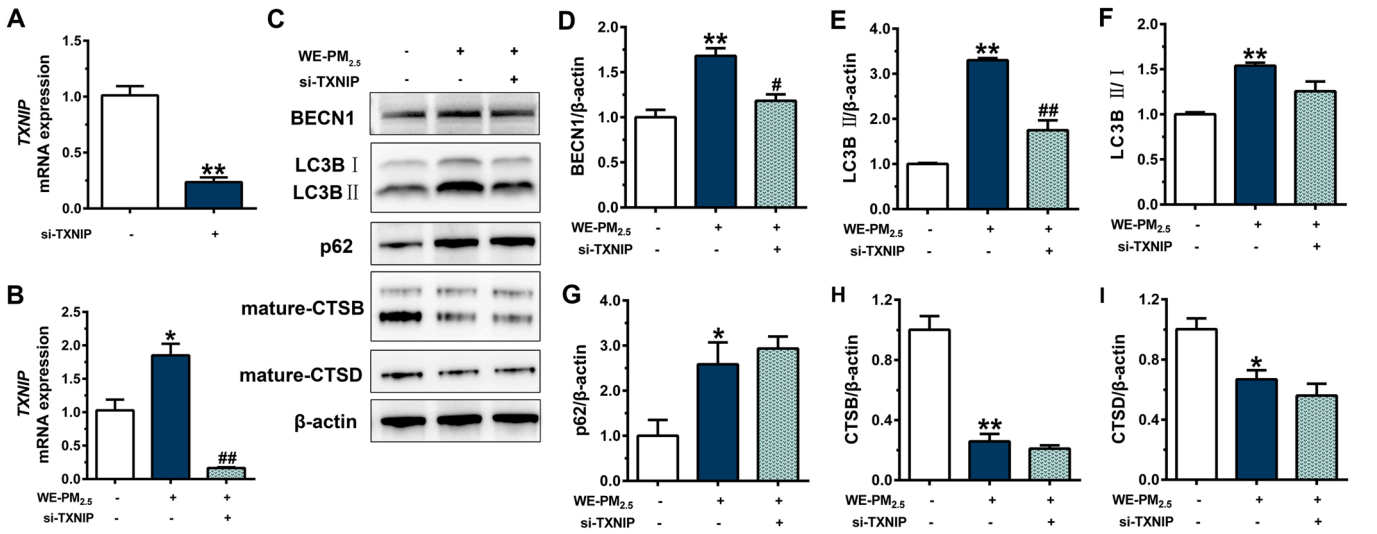

Fig. 7. Effect of inhibition of TXNIP on WE-$PM_{2.5}$-induced autophagy in HUVEC cells. (A-B) Quantitative RT-PCR analysis of *TXNIP* mRNA (C) Western blot analysis of BECN1, LC3B I, LC3B II, p62, CTSB and CTSD protein. (D-I) Quantification of relative protein levels of BECN1(D), LC3B II (E) LC3B II/LC3B I (F), p62 (G), CTSB (H) and CTSD (I). For A, HUVECs were transfected with siRNA control or siRNA TXNIP, respectively; and for B-I, cells were transfected with siRNA control or siRNA TXNIP and exposed to 50 μg/mL of WE-$PM_{2.5}$. $^{*}p < 0.05$, $^{**}p < 0.001$ vs. controls. $^{\#}p < 0.05$, $^{\#\#}p < 0.001$ vs. WE-$PM_{2.5}$-treated cells.

complex; LC3B converts from LC3B I to the lipid-conjugated form LC3B II, which is localized in the autophagosomal membrane and participates in the elongation and formation of autophagosomes; and p62, as an essential substrate, is negatively correlated with the degradation capacity of autophagy [25,27,28]. In this study, 5, 25, and 50 μg/mL of WE-$PM_{2.5}$ resulted in a significant increase in the protein expression of LC3B II and the ratios of LC3B II/LC3B I, suggesting real-world $PM_{2.5}$ from Shanghai, China induced massive accumulation of autophagosomes in HUVEC cells. In fact, autophagosomes accumulation was caused either by autophagy induction or by the inhibition of autophagic degradation. Our results found that both BECN1 and p62 expression were concentration-dependently upregulated in WE-$PM_{2.5}$-exposed HUVEC cells, indicating that WE-$PM_{2.5}$ not only induced the initiation and formation of autophagosomes, but also inhibited the degradation of autophagy. Moreover, the mCherry-GFP-LC3 lentivirus transfection assay further confirmed that 50 μg/mL of WE-$PM_{2.5}$ indeed inhibited the levels of autophagic flux in HUVEC cells due to the blockage of autophagic degradation. Recently, a few studies also confirmed the inhibitory effect of $PM_{2.5}$ on autophagy flux in different human-derived cells, including HUVEC cells [60], human endothelial (EA.hy926) cells [61], human bronchial epithelial (HBE) cells [65] and pheochromocytoma (PC12) cells [59].

The reference ranges of some important metal elements (Al, Mn, Cu, Zn, As, Se, Rb, Ba, and Pb) in the plasma of healthy volunteers were 1.2–17.3, 0.63–2.26, 794–2023, 551–925, 4.4–14.2, 79–141, 101–358, 90–154, and 0.014–0.25 μg/L, respectively [20]. Of these, the metals with the highest levels were Cu and Zn, which were essentially involved in the physiological and biochemical processes in humans. For example, Zn participated in the synthesis of hormones [52,54], and Cu formed part of enzymes [45]. Unfortunately, long-term environmental exposure resulted in abnormal concentrations of trace metals, especially heavy metals in human bodies, which in turn posed a potential health risk. Lan et al. pointed out that ambient $PM_{2.5}$ concentrations were positively associated with serum Mn and As levels and blood pressure in women of childbearing age from Hebei province, China, and serum Mo levels were significantly correlated with systolic blood pressure [29]. In a case-crossover study of Canadian adults, acute cardiovascular events in men were strongly associated with the joint concentrations of both transition metals (Fe, Cu, and Zn) and S content [64]. Notably, accumulating evidence have confirmed that many metals, such as Cu, Zn, Mn, Fe, Cr, Pb, and As, were involved in the process of autophagy in organisms [8,43]. Zn treatment could activate autophagy in mice after spinal cord injury via adenosine 5′-monophosphate (AMP)-activated protein kinase (AMPK)/mTOR signaling [33]. Conversely, Mn exposure blocked TFEB (transcription factor EB) nuclear translocation, thereby leading to the inhibition of autophagic flux which was related to mitochondrial dysfunction in astrocytes [71]. Interestingly, As (Arsenic) exposure not only induced the autophagosome formation through Beclin1-Vps34/PI3K (phosphatidylinositol-4,5-bisphosphate 3-kinase catalytic subunit beta) complex and mTOR pathway, but also impaired the lysosomal function, which in turn blocked autophagosome degradation in mouse testis leydig tumor (MLTC-1) cells [31].

It is not known so far, however, whether or how metals adsorbed in $PM_{2.5}$ participate in the process of autophagic flux and further induce toxic effects. In order to solve this problem, we specially designed two additional exposure groups as supplementary experiments. One was the exposure group of metals-chelated solution which removed 93.35 % of the metals in WE-$PM_{2.5}$; the other was the exposure group of artificial metals mixture to mimic the main metal elements in 50 μg/mL of WE-$PM_{2.5}$, including Fe, Mn, Cr, Cu, V, Zn, Al, Sr, Ba, Pb and As. Our *in vitro* results confirmed that the increasing trend of WE-$PM_{2.5}$-induced BECN1 and LC3B II expression was significantly alleviated after metals were removed, while exposure to artificial metals mixture reproduced the WE-$PM_{2.5}$ effect, suggesting that WE-$PM_{2.5}$-adsorbed major metals were the dominant trigger for the autophagosome initiation and formation. Also, it was the main metals of WE-$PM_{2.5}$ that prevented the degradation process of autophagy, thereby inhibiting the overall autophagic flux in HUVEC cells. Because removal of metals by chelation fully reversed p62 expression induced by WE-$PM_{2.5}$, whereas exposure to artificial metals mixture dramatically increased the protein expression of p62; furthermore, mCherry-GFP-LC3 lentivirus transfection assays verified that there were more autolysosomes than autophagosomes in Chel treatment, however, autophagosomes were dominant over autolysosomes in WE-$PM_{2.5}$ and AMM treatment in HUVEC cells. Indeed, metals played an important role in the toxic effects of atmospheric particulate matters. In our previous study, removal of metals abrogated PM_{10}-induced migration and invasion in A549 cells via LIN28B (lin-28 homolog B)–IL6 (interleukin 6)–STAT3 (signal transducer and activator of transcription 3) axis [42]. Similarly, in an *in vivo* mouse model, the dissolved metals (such as Cu, Fe, Mn, V, Ni, and Cr) that were adsorbed in PM collected near roadways were largely responsible for the pulmonary inflammation and oxidative stress [47]. To our knowledge, this is the first study to

confirm that metals absorbed in real-world $PM_{2.5}$ are primarily responsible for the formation of autophagosomes and inhibition of autophagic flux in HUVEC cells.

The final and crucial step of autophagy is the fusion of the lysosomes with autophagosomes for degradation of cellular waste. The activity and function of lysosomes directly determine whether the process of autophagy can proceed smoothly [44]. Once lysosomes are damaged, the process of autophagic flux will be hindered, resulting in undesired physiological and pathological consequences. It has been reported that different types of particles, especially nanoparticles (such as polystyrene nanoparticles, copper oxide nanoparticles, and silica nanoparticle) impaired the function and integrity of lysosomes, therefore blocked autophagic flux to lead to cardiovascular damage [1,16,70]. Also, researchers have paid special attention to the lysosomal impairment as an emerging toxic mechanism of $PM_{2.5}$. Wang et al. confirmed that exposure to 20 μg/cm^2 of PM SRM1648 for 24 h induced lysosomal alkalization in HUVEC and EA. hy926 cells, evidenced by decreased fluorescence intensity of LysoSensor™ green DND-189 which was a pH-sensitive probe for showing stronger fluorescence in more acidic lysosomal microenvironment [60,61]. Conversely, in this study, the fluorescence intensity significantly increased in response to 50 μg/mL of WE-$PM_{2.5}$ for 48 h in HUVEC cells, indicating the lysosome microenvironment in the presence of WE-$PM_{2.5}$ was more acidic compared to control. This might be due to the fact that WE-$PM_{2.5}$ itself we used was acidic (pH=4.40). The acidic WE-$PM_{2.5}$ was taken up by HUVEC cells and accumulated in the lysosomes, which might lead to the stronger acidity in lysosomal microenvironment. In addition, we found that acidic AMM solution (pH=4.74) also induced lysosomal acidification in HUVEC cells, while the Chel solution (pH=6.24) attenuated the enhanced acidity of lysosomes induced by WE-$PM_{2.5}$. Likewise, a previous study also found that 240 μg/mL of $PM_{2.5}$ collected from Shandong, China resulted in lysosomal acidification in human bronchial epithelial cells (16HBE), evidenced by stained by an acridine orange probe [53]. Accompanied by lysosomal acidification, in this study, the activity of acid phosphatase was weakened, and the protein expression of two key hydrolytic proteases (CTSB and CTSD) was decreased following exposure to 50 μg/mL of WE-$PM_{2.5}$, indicating the degradative capacity of the lysosome was disrupted, thereby inhibiting the autophagic flux caused by WE-$PM_{2.5}$. These outcomes were consistent with recent reports discussing the effect of $PM_{2.5}$ on lysosomes [60,61]. Whether metals from $PM_{2.5}$ were involved in lysosome damage was also our focus. Su et al. dissolved the $PM_{2.5}$ samples in nitric acid and perchloric acid, filtered, dried and distilled to obtain $PM_{2.5}$-metal which subsequently was exposed to HUVEC cells, and found that $PM_{2.5}$-metal was taken up through micropinocytosis-mediated pathway and caused a significant decrease in the mRNA levels of lysosome membrane proteins *LAMP2* and *LAMP3* (lysosomal associated membrane protein 3) [55]. Similarly, in the current study, removal of metals by chelation alleviated lysosome impairment in HUVEC cells, while the artificial metal mixture reproduced this response to WE-$PM_{2.5}$, which was manifested by the changes of lysosome size and acidity, acid phosphatase activity, as well as CTSB and CTSD protein expression. Collectively, it is reasonable to conclude that the impairment of lysosome function caused by WE-$PM_{2.5}$ is largely attributed to the metals with high concentrations in our $PM_{2.5}$ samples.

Oxidative stress is well recognized as an indispensable driver of endothelial dysfunction, resulting in vascular damage and CVD [67]. Various environmental pollutants entering the circulatory system could generate excessive ROS in endothelial cells, such as silica nanoparticles [34], zinc oxide nanoparticles [49], polychlorinated biphenyl (PCB) 118 [38] and $PM_{2.5}$ [62]. Our results also found that exposure to 50 μg/mL WE-$PM_{2.5}$ triggered massive ROS production in HUVEC cells. Importantly, high levels of ROS could not only activate the initiation and formation of autophagosomes, but also suppress the degradation of autophagy by affecting the function of lysosomes, thereby contributing to the blockage of autophagic flux caused by WE-$PM_{2.5}$, which was evidenced by the results that the ROS scavenger reversed WE-$PM_{2.5}$-induced autophagy-related protein expression, including BECN1, LC3B, p62, CTSB and CTSD. In light of the critical status of ROS in autophagy dysregulation, it is necessary to detect ROS-mediated markers for expanding our understanding of the molecular mechanism of $PM_{2.5}$-induced endothelial injury. Previous work has proposed that TXNIP is an important molecular linking between oxidative stress and inflammation in cardiovascular events [14,35]. Under oxidative stress status, the accumulation of ROS facilitated TXNIP-TRX (thioredoxin) dissociation to generate more dissociative TXNIP, thereby activating the NLR family pyrin domain containing 3 (NLRP3) inflammasome to induce the secretion of mature interleukin 1 beta (IL-1β) and interleukin 18 (IL-18). More recently, TXNIP has attracted much interest as an emerging mechanism in regulating autophagy. For example, overexpression of TXNIP activated autophagy in the rat müller cell of diabetic retinopathy through inhibition of the PI3K/AKT (AKT serine/threonine kinase 1)/mTOR signaling pathway [3]. Similarly, Ding et al. also found that exposure of HUVEC cells to the cooking oil fumes-derived $PM_{2.5}$ (COFs-derived $PM_{2.5}$) decreased the phosphorylation of PI3K, AKT, and mTOR, and increased the expression of BECN1 and LC3II, which was effectively reversed by the co-treatment with an antioxidant N-acetyl cysteine (NAC), suggesting that the high levels of ROS induced by COFs-derived $PM_{2.5}$ inhibited the PI3K/AKT/mTOR pathway, thereby promoting the initiation and formation of autophagosomes in HUVEC cells [12]. In this study, WE-$PM_{2.5}$-induced high levels of TXNIP promoted autophagosome initiation and formation, since inhibition of TXNIP expression reversed the increased expression of BECN1 and LC3B caused by WE-$PM_{2.5}$ in HUVEC cells. We speculate that TXNIP, as the downstream molecule of ROS, might promote the autophagosome initiation and formation through targeting the PI3K/AKT/mTOR signaling. In addition, we also found that there was no significant difference in the protein expression of p62 following knockdown of TXNIP in WE-$PM_{2.5}$-exposed cells, indicating TXNIP was not involved in the process of autophagic degradation. This may be explained by the observation that TXNIP failed to affect the degradation capacity of lysosomes, as evidenced by the unchanged expression of CTSB and CTSD after TXNIP was inhibited in HUVEC cells. Taken together, in this case WE-$PM_{2.5}$-induced ROS regulated the entire process of autophagic flux in HUVEC cells, and as the downstream molecule of ROS, TXNIP only participated in the initiation and formation of autophagosomes, but not autophagic degradation.

5. Conclusion

In summary, exposure to water-extracted $PM_{2.5}$ in HUVEC cells not only induced the initiation and formation of autophagosomes, but also impaired lysosomal function, which in turn inhibited autophagic degradation, resulting in the blockage of the entire autophagic flux. More importantly, high levels of metals present in $PM_{2.5}$ collected from Shanghai, China made a significant contribution to WE-$PM_{2.5}$-mediated autophagic flux blockage. This conclusion was verified by the observation that removal of metals by chelation did not lead to the same autophagic effects as the metals-rich WE-$PM_{2.5}$, while the artificial metals mixture reproduced the response induced by WE-$PM_{2.5}$. Mechanistically, high levels of ROS promoted autophagosome initiation and formation by positively regulating TXNIP; however, it was ROS, not TXNIP, that contributed to lysosome impairment, consequently inhibiting autophagic degradation in WE-$PM_{2.5}$-exposed HUVEC cells. Thus, the current study provided new insights into the potential important role of ROS and TXNIP in autophagic flux blockage caused by metal-rich $PM_{2.5}$ from real-world environments in vascular endothelial cells.

CRediT authorship contribution statement

Qingyu Huang: Conceptualization, Supervision, Writing - review &editing, Funding acquisition; **Yan-Yang Lu**: Conceptualization,

Investigation, Visualization, Formal analysis, Methodology, Writing - original draft; Writing - review &editing, Funding acquisition; **Meiyi Cao**: Investigation, Methodology, Visualization; **Fuping Li:** Methodology; **Hongyun Ren**: Investigation; **Qiaoqiao Chi**: Investigation; **Meiping Tian**: Investigation.

Declaration of Competing Interest

The authors declare that they have no known competing financial interests or personal relationships that could have appeared to influence the work reported in this paper.

Data Availability

Data will be made available on request.

Acknowledgements

We thank Prof. Jinsheng Chen (Institute of Urban Environment, Chinese Academy of Sciences) for kindly donating the $PM_{2.5}$ samples. Qingyu Huang and Yan-yang Lu receive financial support from the National Natural Science Foundation of China, China [22076179 and 42007387], and Beijing Key Laboratory of Environmental Toxicology, China [2022hjd103].

Environmental implication

Up to now, more than 50 % of the total population worldwide is exposed to high levels of fine particulate matter ($PM_{2.5}$). $PM_{2.5}$ pollution is still a top 10 environmental risk factor for public health, and one of the largest threats to human health is to exacerbate the pathogenesis of cardiovascular diseases. However, major toxic components and underlying mechanism remain unclear. In this study, we explored the toxic mechanism of $PM_{2.5}$ in vascular endothelial cells from the perspective of autophagy, and confirmed the important role of metal components, which provide basic knowledge for finding new targets of $PM_{2.5}$-induced vascular endothelial injury.

Appendix A. Supporting information

Supplementary data associated with this article can be found in the online version at doi:10.1016/j.jhazmat.2022.130623.

References

[1] Abulikemu, A., Zhao, X., Qi, Y., Liu, Y., Wang, J., Zhou, W., et al., 2022. Lysosomal impairment-mediated autophagy dysfunction responsible for the vascular endothelial apoptosis caused by silica nanoparticle via ROS/PARP1/AIF signaling pathway. Environ Pollut 304, 119202. https://doi.org/10.1016/j.envpol.2022.119202.

[2] Alves, C.A., Vicente, A.M., Custódio, D., Cerqueira, M., Nunes, T., Pio, C., et al., 2017. Polycyclic aromatic hydrocarbons and their derivatives (nitro-PAHs, oxygenated PAHs, and azaarenes) in $PM_{2.5}$ from Southern European cities. Sci Total Environ 595, 494–504. https://doi.org/10.1016/j.scitotenv.2017.03.256.

[3] Ao, H., Li, H., Zhao, X., Liu, B., Lu, L., 2021. TXNIP positively regulates the autophagy and apoptosis in the rat müller cell of diabetic retinopathy. Life Sci 267, 118988. https://doi.org/10.1016/j.lfs.2020.118988.

[4] Bio-Rad Laboratories, 1998. Chelex®100 and Chelex 20 chelating ion exchange resin instruction manual. Bio-Rad Laboratories.

[5] Bu, X., Xie, Z., Liu, J., Wei, L., Wang, X., Chen, M., et al., 2021. Global $PM_{2.5}$-attributable health burden from 1990 to 2017: estimates from the global burden of disease study 2017. Environ Res 197, 111123. https://doi.org/10.1016/j.envres.2021.111123.

[6] Callén, M.S., Iturmendi, A., López, J.M., 2014. Source apportionment of atmospheric $PM_{2.5}$-bound polycyclic aromatic hydrocarbons by a PMF receptor model. Assessment of potential risk for human health. Environ Pollut 195, 167–177. https://doi.org/10.1016/j.envpol.2014.08.025.

[7] Cao, C., Jiang, W., Wang, B., Fang, J., Lang, J., Tian, G., et al., 2014. Inhalable microorganisms in Beijing's $PM_{2.5}$ and PM_{10} pollutants during a severe smog event. Environ Sci Technol 48 (3), 1499–1507. https://doi.org/10.1021/es4048472.

[8] Chatterjee, S., Sarkar, S., Bhattacharya, S., 2014. Toxic metals and autophagy. Chem Res Toxicol 27 (11), 1887–1900. https://doi.org/10.1021/tx500264s.

[9] Cohen, A.J., Brauer, M., Burnett, R., Anderson, H.R., Frostad, J., Estep, K., et al., 2017. Estimates and 25-year trends of the global burden of disease attributable to ambient air pollution: an analysis of data from the Global Burden of Diseases Study 2015. Lancet 389 (10082), 1907–1918. https://doi.org/10.1016/s0140-6736(17)30505-6.

[10] Collaborators, G.V., 2020. Five insights from the Global Burden of Disease Study 2019. Lancet 396 (10258), 1135–1159. https://doi.org/10.1016/s0140-6736(20)31404-5.

[11] Cuevas, A.K., Niu, J., Zhong, M., Liberda, E.N., Ghio, A., Qu, Q., et al., 2015. Metal rich particulate matter impairs acetylcholine-mediated vasorelaxation of microvessels in mice. Part Fibre Toxicol 12, 14. https://doi.org/10.1186/s12989-014-0077-x.

[12] Ding, R., Zhang, C., Zhu, X., Cheng, H., Zhu, F., Xu, Y., et al., 2017. ROS-AKT-mTOR axis mediates autophagy of human umbilical vein endothelial cells induced by cooking oil fumes-derived fine particulate matters in vitro. Free Radic Biol Med 113, 452–460. https://doi.org/10.1016/j.freeradbiomed.2017.10.386.

[13] Domingues, A., Boisson-Vidal, C., Marquet de Rouge, P., Dizier, B., Sadoine, J., Mignon, V., et al., 2020. Targeting endothelial thioredoxin-interacting protein (TXNIP) protects from metabolic disorder-related impairment of vascular function and post-ischemic revascularisation. Angiogenesis 23 (2), 249–264. https://doi.org/10.1007/s10456-019-09704-x.

[14] Domingues, A., Jolibois, J., Marquet de Rougé, P., Nivet-Antoine, V., 2021. The emerging role of TXNIP in ischemic and cardiovascular diseases; a novel marker and therapeutic target. Int. J. Mol. Sci. 22 (4), 1693. https://doi.org/10.3390/ijms22041693.

[15] Dominici, F., Peng, R.D., Bell, M.L., Pham, L., McDermott, A., Zeger, S.L., et al., 2006. Fine particulate air pollution and hospital admission for cardiovascular and respiratory diseases. JAMA 295 (10), 1127–1134. https://doi.org/10.1001/jama.295.10.1127.

[16] Fröhlich, E., Meindl, C., Roblegg, E., Ebner, B., Absenger, M., Pieber, T.R., 2012. Action of polystyrene nanoparticles of different sizes on lysosomal function and integrity. Part Fibre Toxicol 9, 26. https://doi.org/10.1186/1743-8977-9-26.

[17] Gao, C., Wang, R., Li, B., Guo, Y., Yin, T., Xia, Y., et al., 2020. TXNIP/Redd1 signalling and excessive autophagy: a novel mechanism of myocardial ischaemia/reperfusion injury in mice. Cardiovasc Res 116 (3), 645–657. https://doi.org/10.1093/cvr/cvz152.

[18] Gao, P., Lei, T., Jia, L., Song, Y., Lin, N., Du, Y., et al., 2017. Exposure and health risk assessment of $PM_{2.5}$-bound trace metals during winter in university campus in Northeast China. Sci Total Environ 576, 628–636. https://doi.org/10.1016/j.scitotenv.2016.10.126.

[19] Gimbrone Jr., M.A., García-Cardeña, G., 2016. Endothelial cell dysfunction and the pathobiology of atherosclerosis. Circ Res 118 (4), 620–636. https://doi.org/10.1161/circresaha.115.306301.

[20] Goullé, J.P., Mahieu, L., Castermant, J., Neveu, N., Bonneau, L., Lainé, G., et al., 2005. Metal and metalloid multi-elementary ICP-MS validation in whole blood, plasma, urine and hair. Ref Values Forensic Sci Int 153 (1), 39–44. https://doi.org/10.1016/j.forsciint.2005.04.020.

[21] Han, H., Liu, L., Chen, M., Liu, Y., Wang, H., Chen, L., 2020. The optimal compound reference genes for qRT-PCR analysis in the developing rat long bones under physiological conditions and prenatal dexamethasone exposure model. Reprod Toxicol 98, 242–251. https://doi.org/10.1016/j.reprotox.2020.10.008.

[22] Han, X., Alam, M.N., Cao, M., Wang, X., Cen, M., Tian, M., et al., 2022. Low levels of perfluorooctanoic acid exposure activates steroid hormone biosynthesis through repressing histone methylation in rats. Environ Sci Technol 56 (9), 5664–5672. https://doi.org/10.1021/acs.est.1c08885.

[23] Hayes, R.B., Lim, C., Zhang, Y., Cromar, K., Shao, Y., Reynolds, H.R., et al., 2020. $PM_{2.5}$ air pollution and cause-specific cardiovascular disease mortality. Int J Epidemiol 49 (1), 25–35. https://doi.org/10.1093/ije/dyz114.

[24] Heo, J., Antkiewicz, D.S., Shafer, M.M., Perkins, D.A., Sioutas, C., Schauer, J.J., 2015. Assessing the role of chemical components in cellular responses to atmospheric particle matter (PM) through chemical fractionation of PM extracts. Anal Bioanal Chem 407 (20), 5953–5963. https://doi.org/10.1007/s00216-015-8749-4.

[25] Hill, S.M., Wrobel, L., Rubinsztein, D.C., 2019. Post-translational modifications of Beclin 1 provide multiple strategies for autophagy regulation. Cell Death Differ 26 (4), 617–629. https://doi.org/10.1038/s41418-018-0254-9.

[26] Huang, C., Zhang, Y., Kelly, D.J., Tan, C.Y., Gill, A., Cheng, D., et al., 2016. Thioredoxin interacting protein (TXNIP) regulates tubular autophagy and mitophagy in diabetic nephropathy through the mTOR signaling pathway. Sci Rep 6, 29196. https://doi.org/10.1038/srep29196.

[27] Kim, K.H., Lee, M.S., 2014. Autophagy–a key player in cellular and body metabolism. Nat Rev Endocrinol 10 (6), 322–337. https://doi.org/10.1038/nrendo.2014.35.

[28] Klionsky, D.J., Abdel-Aziz, A.K., Abdelfatah, S., Abdellatif, M., Abdoli, A., Abel, S., et al., 2021. Guidelines for the use and interpretation of assays for monitoring autophagy (4th edition)[1]. Autophagy 17 (1), 1–382. https://doi.org/10.1080/15548627.2020.1797280.

[29] Lan, C., Liu, Y., Li, Q., Wang, B., Xue, T., Chen, J., et al., 2021. Internal metal(loid)s are potentially involved in the association between ambient fine particulate matter and blood pressure: A repeated-measurement study in north China. Chemosphere 267, 129146. https://doi.org/10.1016/j.chemosphere.2020.129146.

[30] Li, X., Sun, X., Carmeliet, P., 2019. Hallmarks of endothelial cell metabolism in health and disease. Cell Metab 30 (3), 414–433. https://doi.org/10.1016/j.cmet.2019.08.011.

[31] Liang, C., Feng, Z., Manthari, R.K., Wang, C., Han, Y., Fu, W., et al., 2020. Arsenic induces dysfunctional autophagy via dual regulation of mTOR pathway and

Beclin1-Vps34/PI3K complex in MLTC-1 cells. J Hazard Mater 391, 122227. https://doi.org/10.1016/j.jhazmat.2020.122227.
[32] Liang, S., Zhang, J., Ning, R., Du, Z., Liu, J., Batibawa, J.W., et al., 2020. The critical role of endothelial function in fine particulate matter-induced atherosclerosis. Part Fibre Toxicol 17 (1), 61. https://doi.org/10.1186/s12989-020-00391-x.
[33] Lin, S., Tian, H., Lin, J., Xu, C., Yuan, Y., Gao, S., et al., 2020. Zinc promotes autophagy and inhibits apoptosis through AMPK/mTOR signaling pathway after spinal cord injury. Neurosci Lett 736, 135263. https://doi.org/10.1016/j.neulet.2020.135263.
[34] Liu, X., Lu, B., Fu, J., Zhu, X., Song, E., Song, Y., 2021. Amorphous silica nanoparticles induce inflammation via activation of NLRP3 inflammasome and HMGB1/TLR4/MYD88/NF-kb signaling pathway in HUVEC cells. J. Hazard. Mater. 404, 124050 https://doi.org/10.1016/j.jhazmat.2020.124050.
[35] Liu, Y., Lian, K., Zhang, L., Wang, R., Yi, F., Gao, C., et al., 2014. TXNIP mediates NLRP3 inflammasome activation in cardiac microvascular endothelial cells as a novel mechanism in myocardial ischemia/reperfusion injury. Basic Res Cardiol 109 (5), 415. https://doi.org/10.1007/s00395-014-0415-z.
[36] Liu, Z., Leng, W., Zhang, J., Zhang, G., Liu, D., Zhao, Z., et al., 2022. miR-146a-5p/TXNIP axis attenuates intestinal ischemia-reperfusion injury by inhibiting autophagy via the PRKAA/mTOR signaling pathway. Biochem Pharmacol 197, 114839. https://doi.org/10.1016/j.bcp.2021.114839.
[37] Livak, K.J., Schmittgen, T.D., 2001. Analysis of relative gene expression data using real-time quantitative PCR and the $2^{-\Delta\Delta CT}$ Method. Methods 25 (4), 402–408. https://doi.org/10.1006/meth.2001.1262.
[38] Long, Y., Liu, X., Tan, X.Z., Jiang, C.X., Chen, S.W., Liang, G.N., et al., 2020. ROS-induced NLRP3 inflammasome priming and activation mediate PCB 118- induced pyroptosis in endothelial cells. Ecotoxicol Environ Saf 189, 109937. https://doi.org/10.1016/j.ecoenv.2019.109937.
[39] Long, Y.M., Yang, X.Z., Yang, Q.Q., Clermont, A.C., Yin, Y.G., Liu, G.L., et al., 2020. $PM_{2.5}$ induces vascular permeability increase through activating MAPK/ERK signaling pathway and ROS generation. J Hazard Mater 386, 121659. https://doi.org/10.1016/j.jhazmat.2019.121659.
[40] Loomis, D., Grosse, Y., Lauby-Secretan, B., El Ghissassi, F., Bouvard, V., Benbrahim-Tallaa, L., et al., 2013. The carcinogenicity of outdoor air pollution. Lancet Oncol 14 (13), 1262–1263. https://doi.org/10.1016/s1470-2045(13)70487-x.
[41] Lu, Y.Y., Li, H., Ren, H., Zhang, X., Huang, F., Zhang, D., et al., 2022. Size-dependent effects of polystyrene nanoplastics on autophagy response in human umbilical vein endothelial cells. J Hazard Mater 421, 126770. https://doi.org/10.1016/j.jhazmat.2021.126770.
[42] Lu, Y.Y., Lin, Y., Ding, D.X., Su, S., Chi, Q.Q., Zhang, Y.C., et al., 2018. MiR-26a functions as a tumor suppressor in ambient particulate matter-bound metal-triggered lung cancer cell metastasis by targeting LIN28B-IL6-STAT3 axis. Arch Toxicol 92 (3), 1023–1035. https://doi.org/10.1007/s00204-017-2141-4.
[43] Luo, Y., Fu, Y., Huang, Z., Li, M., 2021. Transition metals and metal complexes in autophagy and diseases. J Cell Physiol 236 (10), 7144–7158. https://doi.org/10.1002/jcp.30359.
[44] Mahapatra, K.K., Mishra, S.R., Behera, B.P., Patil, S., Gewirtz, D.A., Bhutia, S.K., 2021. The lysosome as an imperative regulator of autophagy and cell death. Cell Mol Life Sci 78 (23), 7435–7449. https://doi.org/10.1007/s00018-021-03988-3.
[45] Meury, M., Knop, M., Seebeck, F.P., 2017. Structural basis for copper-oxygen mediated C-H bond activation by the formylglycine-generating. Enzym Angew Chem Int Ed Engl 56 (28), 8115–8119. https://doi.org/10.1002/anie.201702901.
[46] Münzel, T., Gori, T., Al-Kindi, S., Deanfield, J., Lelieveld, J., Daiber, A., et al., 2018. Effects of gaseous and solid constituents of air pollution on endothelial function. Eur Heart J 39 (38), 3543–3550. https://doi.org/10.1093/eurheartj/ehy481.
[47] Pardo, M., Shafer, M.M., Rudich, A., Schauer, J.J., Rudich, Y., 2015. Single exposure to near roadway particulate matter leads to confined inflammatory and defense responses: possible role of metals. Environ Sci Technol 49 (14), 8777–8785. https://doi.org/10.1021/acs.est.5b01449.
[48] Pope 3rd, C.A., Bhatnagar, A., McCracken, J.P., Abplanalp, W., Conklin, D.J., O'Toole, T., 2016. Exposure to fine particulate air pollution is associated with endothelial injury and systemic inflammation. Circ. Res. 119 (11), 1204–1214. https://doi.org/10.1161/circresaha.116.309279.
[49] Qin, X., Zhang, J., Wang, B., Xu, G., Yang, X., Zou, Z., et al., 2021. Ferritinophagy is involved in the zinc oxide nanoparticles-induced ferroptosis of vascular endothelial cells. Autophagy 17 (12), 4266–4285. https://doi.org/10.1080/15548627.2021.1911016.
[50] Saffari, A., Daher, N., Shafer, M.M., Schauer, J.J., Sioutas, C., 2014. Global perspective on the oxidative potential of airborne particulate matter: a synthesis of research findings. Environ Sci Technol 48 (13), 7576–7583. https://doi.org/10.1021/es500937x.
[51] Saftig, P., Haas, A., 2016. Turn up the lysosome. Nat Cell Biol 18 (10), 1025–1027. https://doi.org/10.1038/ncb3409.
[52] Severo, J.S., Morais, J.B.S., de Freitas, T.E.C., Andrade, A.L.P., Feitosa, M.M., Fontenelle, L.C., et al., 2019. The role of zinc in thyroid hormones metabolism. Int J Vitam Nutr Res 89 (1–2), 80–88. https://doi.org/10.1024/0300-9831/a000262.
[53] Shan, X., Liu, L., Li, G., Xu, K., Liu, B., Jiang, W., 2021. $PM_{2.5}$ and the typical components cause organelle damage, apoptosis and necrosis: role of reactive oxygen species. Sci Total Environ 782, 146785. https://doi.org/10.1016/j.scitotenv.2021.146785.
[54] Smith, G.D., Swenson, D.C., Dodson, E.J., Dodson, G.G., Reynolds, C.D., 1984. Structural stability in the 4-zinc human insulin hexamer. Proc Natl Acad Sci U. S. A. 81 (22), 7093–7097. https://doi.org/10.1073/pnas.81.22.7093.
[55] Su, R., Jin, X., Li, H., Huang, L., Li, Z., 2020. The mechanisms of $PM_{2.5}$ and its main components penetrate into HUVEC cells and effects on cell organelles. Chemosphere 241, 125127. https://doi.org/10.1016/j.chemosphere.2019.125127.
[56] Sun, L., Fu, J., Lin, S.H., Sun, J.L., Xia, L., Lin, C.H., et al., 2020. Particulate matter of 2.5 μm or less in diameter disturbs the balance of T(H)17/regulatory T cells by targeting glutamate oxaloacetate transaminase 1 and hypoxia-inducible factor 1α in an asthma model. J Allergy Clin Immunol 145 (1), 402–414. https://doi.org/10.1016/j.jaci.2019.10.008.
[57] Visentin, M., Pagnoni, A., Sarti, E., Pietrogrande, M.C., 2016. Urban $PM_{2.5}$ oxidative potential: importance of chemical species and comparison of two spectrophotometric cell-free assays. Environ Pollut 219, 72–79. https://doi.org/10.1016/j.envpol.2016.09.047.
[58] Wang, W., Deng, Z., Feng, Y., Liao, F., Zhou, F., Feng, S., et al., 2017. $PM_{2.5}$ induced apoptosis in endothelial cell through the activation of the p53-bax-caspase pathway. Chemosphere 177, 135–143. https://doi.org/10.1016/j.chemosphere.2017.02.144.
[59] Wang, Y., Li, C., Zhang, X., Kang, X., Li, Y., Zhang, W., et al., 2021. Exposure to $PM_{2.5}$ aggravates Parkinson's disease via inhibition of autophagy and mitophagy pathway. Toxicology 456, 152770. https://doi.org/10.1016/j.tox.2021.152770.
[60] Wang, Y., Liu, N., Huang, X., Hu, W., Ma, Y., Liang, Y., et al., 2021. Atmospheric particulate matter impedes autophagic flux by impairing lysosomal milieu and integrity in human umbilical vein endothelial cells (HUVECs. Sci Total Environ 761, 143290. https://doi.org/10.1016/j.scitotenv.2020.143290.
[61] Wang, Y., Ma, Y., Yao, Y., Liu, Q., Pang, Y., Tang, M., 2021. Ambient particulate matter triggers defective autophagy and hijacks endothelial cell renewal through oxidative stress-independent lysosomal impairment. Environ Pollut 286, 117295. https://doi.org/10.1016/j.envpol.2021.117295.
[62] Wang, Y., Tang, M., 2019. $PM_{2.5}$ induces ferroptosis in human endothelial cells through iron overload and redox imbalance. Environ Pollut 254, 112937. https://doi.org/10.1016/j.envpol.2019.07.105.
[63] Wang, Y., Tang, M., 2020. $PM_{2.5}$ induces autophagy and apoptosis through endoplasmic reticulum stress in human endothelial cells. Sci Total Environ 710, 136397. https://doi.org/10.1016/j.scitotenv.2019.136397.
[64] Weichenthal, S., Lavigne, E., Traub, A., Umbrio, D., You, H., Pollitt, K., et al., 2021. Association of sulfur, transition metals, and the oxidative potential of outdoor $PM_{2.5}$ with acute cardiovascular events: a case-crossover study of Canadian adults. Environ Health Perspect 129 (10), 107005. https://doi.org/10.1289/ehp9449.
[65] Wu, Y.F., Li, Z.Y., Dong, L.L., Li, W.J., Wu, Y.P., Wang, J., et al., 2020. Inactivation of MTOR promotes autophagy-mediated epithelial injury in particulate matter-induced airway inflammation. Autophagy 16 (3), 435–450. https://doi.org/10.1080/15548627.2019.1628536.
[66] Xie, W., You, J., Zhi, C., Li, L., 2021. The toxicity of ambient fine particulate matter (PM2.5) to v ascular endothelial cells. J Appl Toxicol 41 (5), 713–723. https://doi.org/10.1002/jat.4138.
[67] Xu, S., Ilyas, I., Little, P.J., Li, H., Kamato, D., Zheng, X., et al., 2021. Endothelial dysfunction in atherosclerotic cardiovascular diseases and beyond: from mechanism to pharmacotherapies. Pharmacol Rev 73 (3), 924–967. https://doi.org/10.1124/pharmrev.120.000096.
[68] Ying, Z., Xu, X., Chen, M., Liu, D., Zhong, M., Chen, L.C., et al., 2013. A synergistic vascular effect of airborne particulate matter and nickel in a mouse model. Toxicol Sci 135 (1), 72–80. https://doi.org/10.1093/toxsci/kft136.
[69] Yu, Z., Wang, H., Zhang, X., Gong, S., Liu, Z., Zhao, N., et al., 2022. Long-term environmental surveillance of PM2.5-bound polycyclic aromatic hydrocarbons in Jinan, China (2014-2020): health risk assessment. J Hazard Mater 425, 127766. https://doi.org/10.1016/j.jhazmat.2021.127766.
[70] Zhang, J., Zou, Z., Wang, B., Xu, G., Wu, Q., Zhang, Y., et al., 2018. Lysosomal deposition of copper oxide nanoparticles triggers HUVEC cells death. Biomaterials 161, 228–239. https://doi.org/10.1016/j.biomaterials.2018.01.048.
[71] Zhang, Z., Yan, J., Bowman, A.B., Bryan, M.R., Singh, R., Aschner, M., 2020. Dysregulation of TFEB contributes to manganese-induced autophagic failure and mitochondrial dysfunction in astrocytes. Autophagy 16 (8), 1506–1523. https://doi.org/10.1080/15548627.2019.1688488.